

# Solvothermal guided V<sub>2</sub>O<sub>5</sub> microspherical nanoparticles constructing high performance aqueous zinc-ion batteries

Xianghui Jia<sup>†</sup>, Kaixi Yan<sup>†</sup>, Yanzhi Sun<sup>†,\*</sup>, Yongmei Chen<sup>†</sup>, Yang Tang<sup>†</sup>, Junqing Pan<sup>‡,\*</sup> and Pingyu Wan<sup>†</sup>

<sup>†</sup>National Fundamental Research Laboratory of New Hazardous Chemicals Assessment and Accident Analysis, Institute of Applied Electrochemistry, Beijing University of Chemical Technology, Beijing 100029, China.

<sup>‡</sup>State Key Laboratory of Chemical Resource Engineering, Beijing University of Chemical Technology, Beijing 100029, China.

\*E-mails: sunyz@buct.edu.cn (Y. Sun); jqpan@buct.edu.cn (J. Pan). Tel./Fax: 8610-64435452.

## Experimental Section

### Materials characterization

The crystal structure of the V<sub>2</sub>O<sub>5</sub> samples were analyzed by X-ray diffraction (XRD) and the morphology and elemental content of V<sub>2</sub>O<sub>5</sub> was investigated by transmission electron microscopy (TEM), scanning electron microscopy (SEM) and X-ray energy spectrometry (EDS). X-ray photoelectron spectroscopy (XPS) was carried out with Thermo Scientific K-Alpha to characterize the surface chemistry of the electrode materials and the valence state of vanadium. Fourier transform infrared spectroscopy (FT-IR) was used to test the chemical bonding and molecular structure of the VOCH precursors and V<sub>2</sub>O<sub>5</sub> samples. The composition and decomposition temperature of the ethanol or glycol complexes in the VOCH precursor were studied by thermogravimetric analysis (TGA/DSC) in an air atmosphere in the temperature range 0~500 °C at a heating rate of 10 °C min<sup>-1</sup>. The specific surface area was determined using a fully automated specific surface area and porosity analyzer according to the Brunner-Emmett-Taylor (BET) method.

### Electrochemical measurement

Charge-discharge cycles of the cells were tested at room temperature using a LAND-CT3002A multi-channel battery test system. Cyclic voltammetry (CV) and electrochemical impedance spectroscopy (EIS) tests were carried out on Zn|V<sub>2</sub>O<sub>5</sub> cells using an electrochemical workstation (CHI 660E) with scanning voltage from 0.4 to 1.4 V and AC impedance test at open circuit voltage.

The diffusion coefficient of Zn<sup>2+</sup> ( $D_{Zn}$ ) was calculated according to the following equation:

$$D_{Zn} = \frac{4L^2}{\pi\tau} \left( \frac{\Delta E_s}{\Delta E_t} \right)^2 \quad (S1)$$

In Equation (S1),  $\tau$  is the pulse duration of the constant current,  $L$  is the Zn<sup>2+</sup> diffusion path,  $\Delta E_s$  is the voltage change of the termination voltage of two adjacent relaxation steps and  $\Delta E_t$  is the voltage difference during the current pulse, subtracting the IR drop.

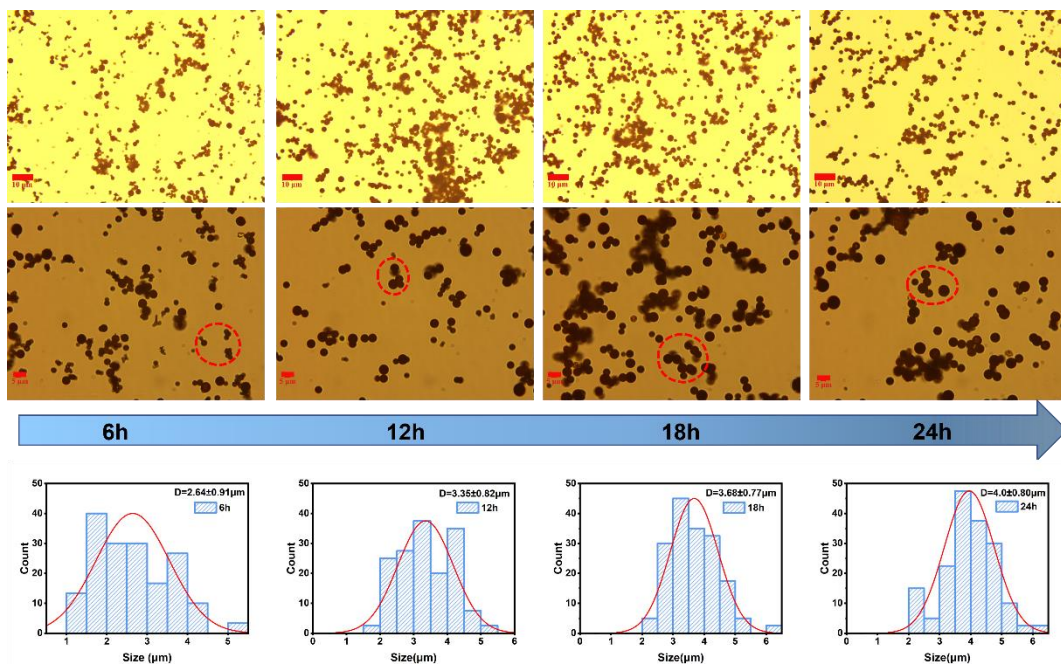


Figure S1. Size of the  $V_2O_5$ -20 microspheres at different reaction times (from 6 h to 24 h).

It can be seen for Figure S1 that the microspheres became larger and more uniform in size as the reaction time increased. The average diameter of the synthesized microspheres was 4 μm at the maximum reaction time of 24 h.

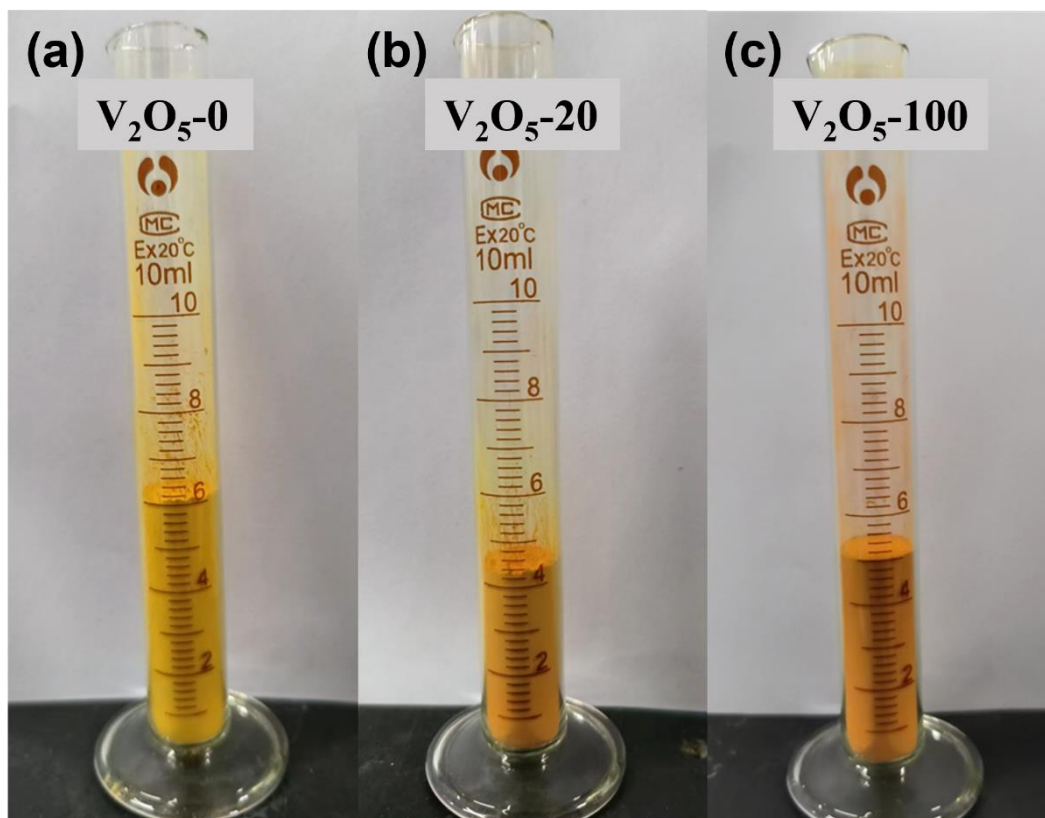


Figure S2. Volume comparison of (a)  $V_2O_5-0$ , (b)  $V_2O_5-20$ , and (c)  $V_2O_5-100$  with the same mass (5 g).

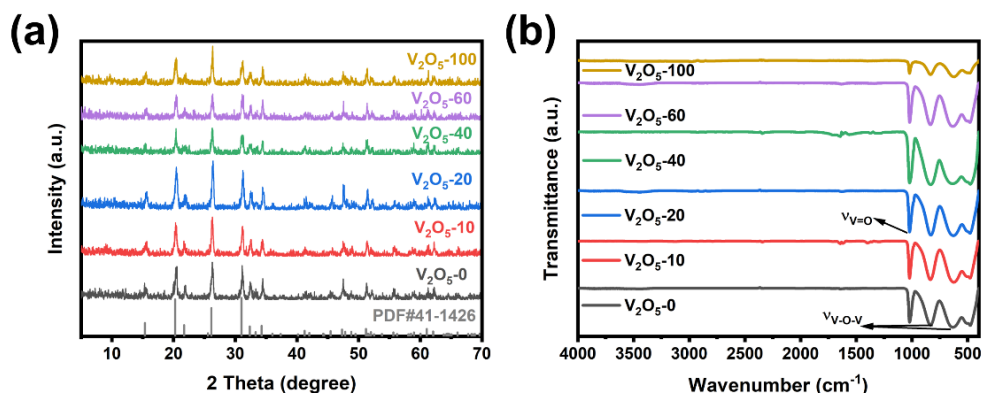


Figure S3. XRD patterns (a) and FT-IR spectra (b) of  $V_2O_5$  samples.

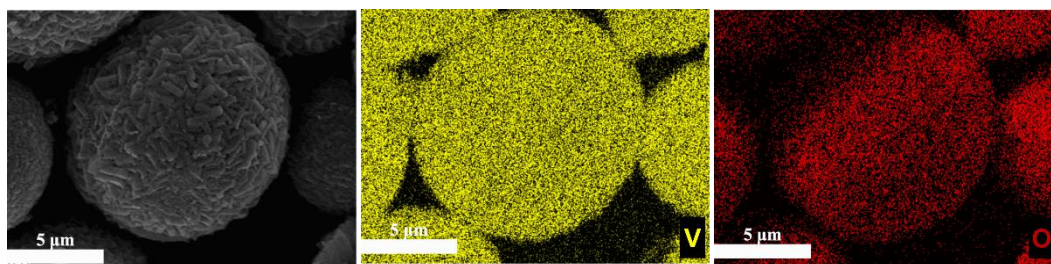


Figure S4. Elemental distribution of  $V_2O_5$ -20.

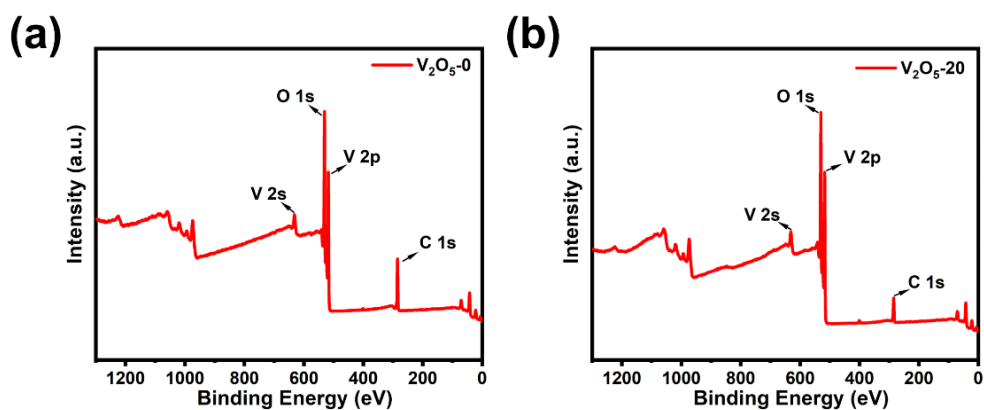


Figure S5. XPS survey spectra of (a)  $V_2O_5$ -0, (b)  $V_2O_5$ -20.

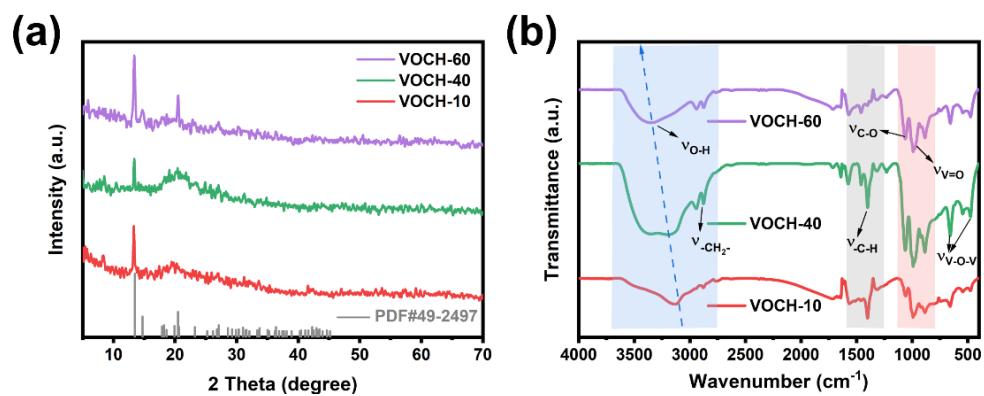


Figure S6. XRD patterns (a) and FT-IR spectra (b) of VOCH precursors.

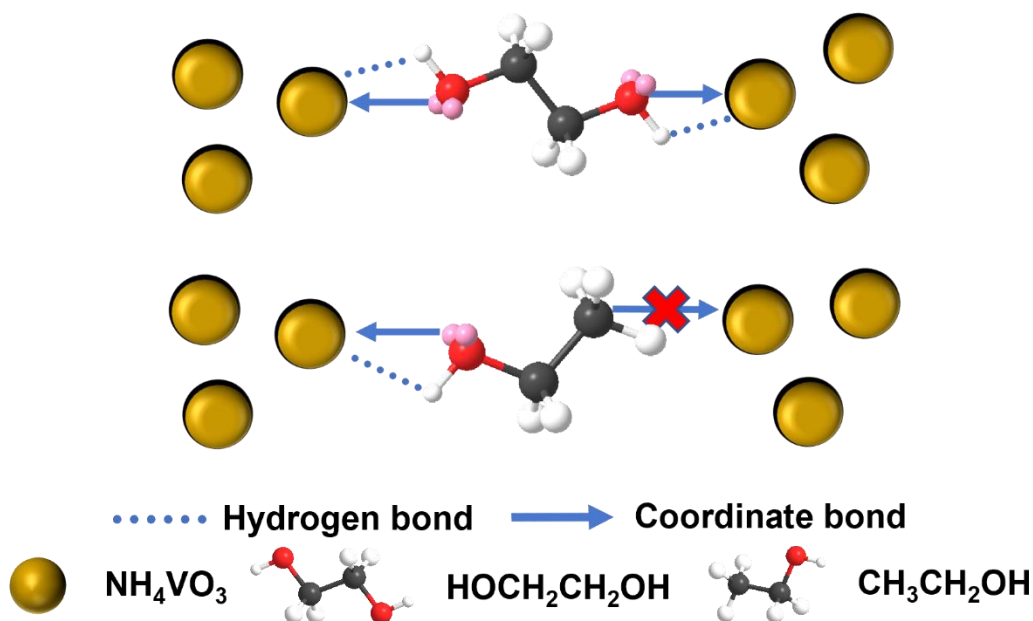


Figure S7. Schematic illustration of the chaining of ethylene glycol or ethanol with nanoparticles.

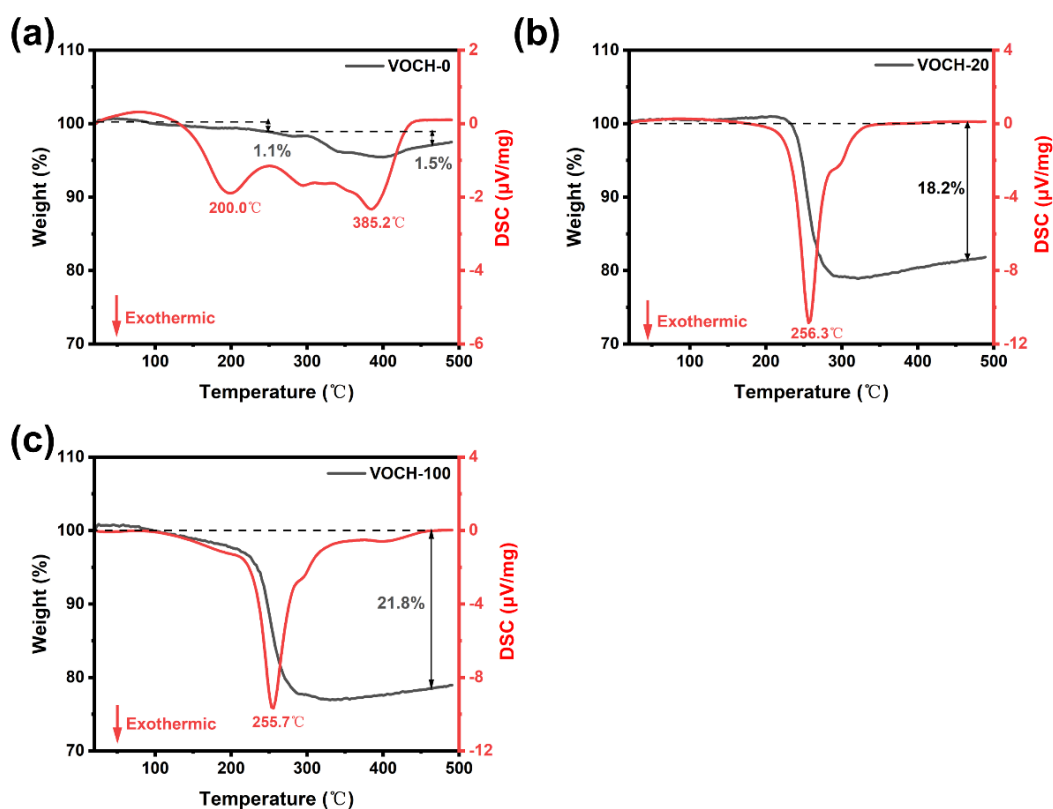


Figure S8. TGA/DSC profiles of (a) VOCH-0, (b) VOCH-20 and (c) VOCH-100 before calcination.

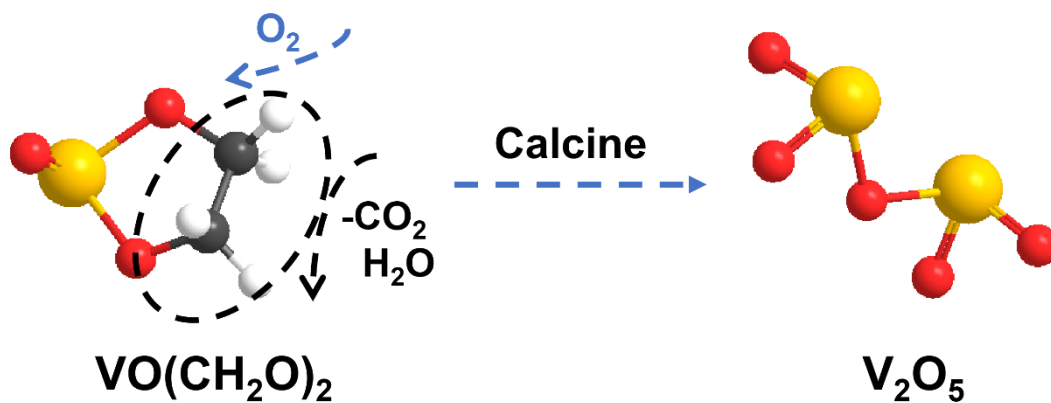


Figure S9. Schematic of  $\text{V}_2\text{O}_5$  formation by calcination of VOCH precursors.

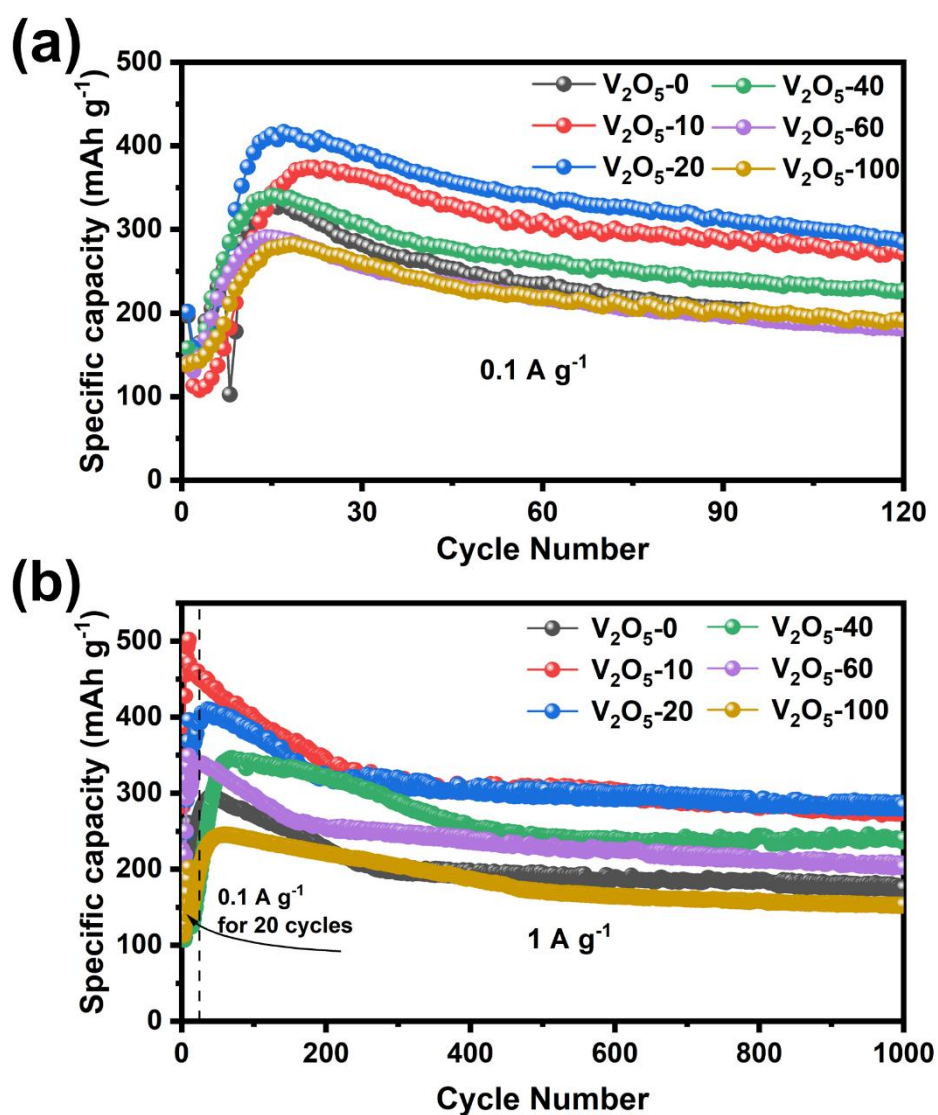


Figure S10. Cycle performance of different  $\text{V}_2\text{O}_5$  electrodes at (a)  $0.1 \text{ A g}^{-1}$ , (b)  $1 \text{ A g}^{-1}$ .

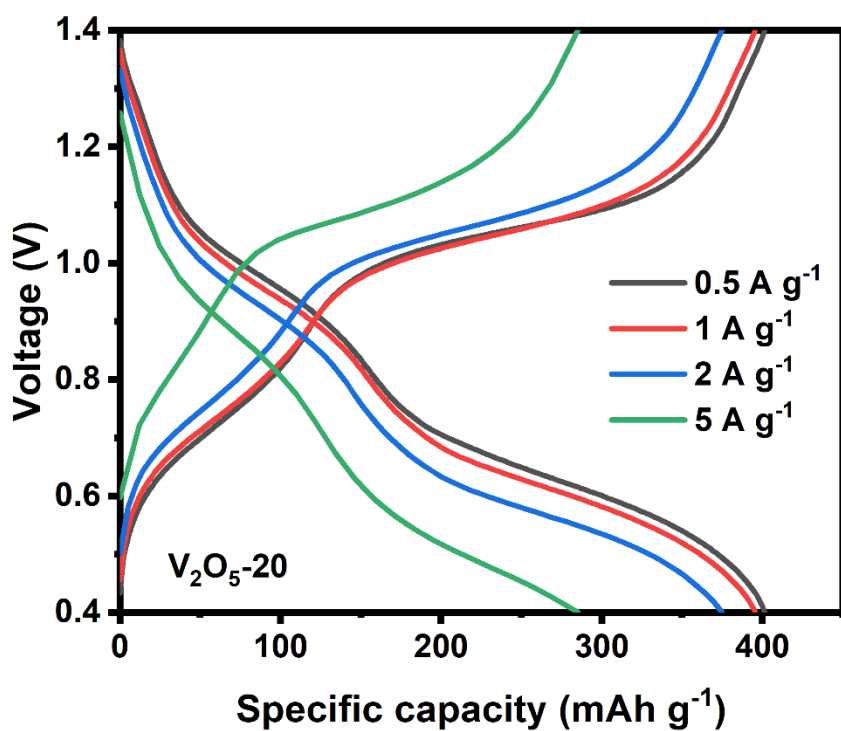


Figure S11. Specific capacity of  $V_2O_5-20$  cathode at various current densities.

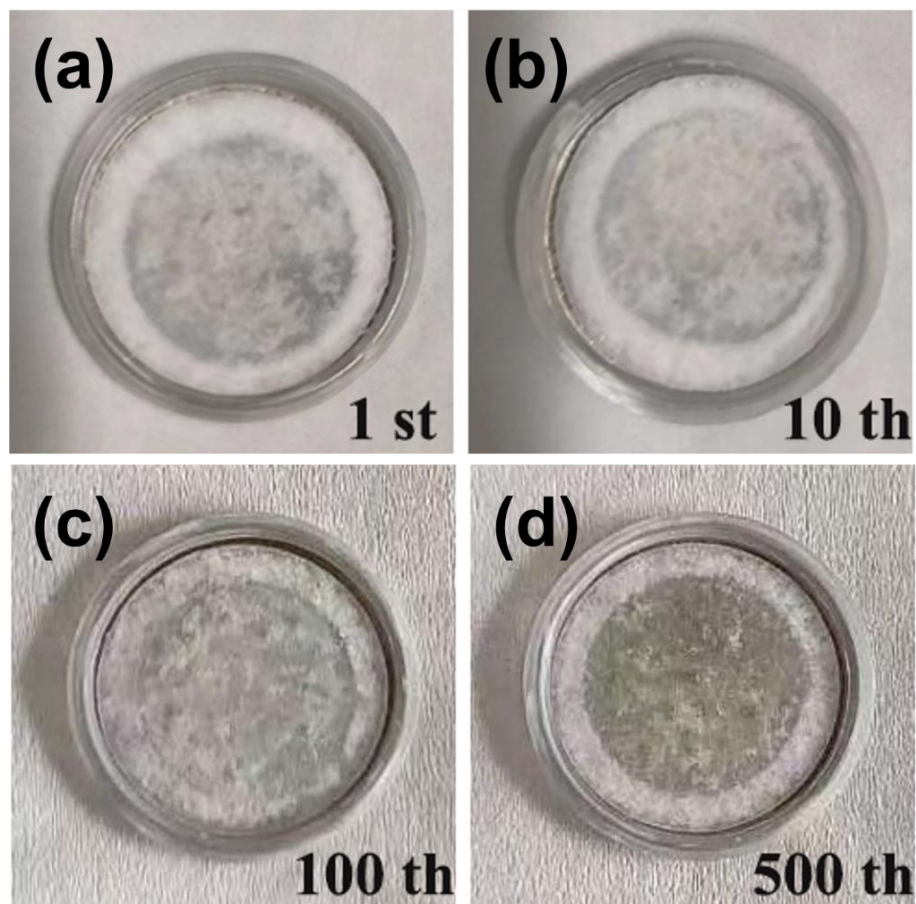
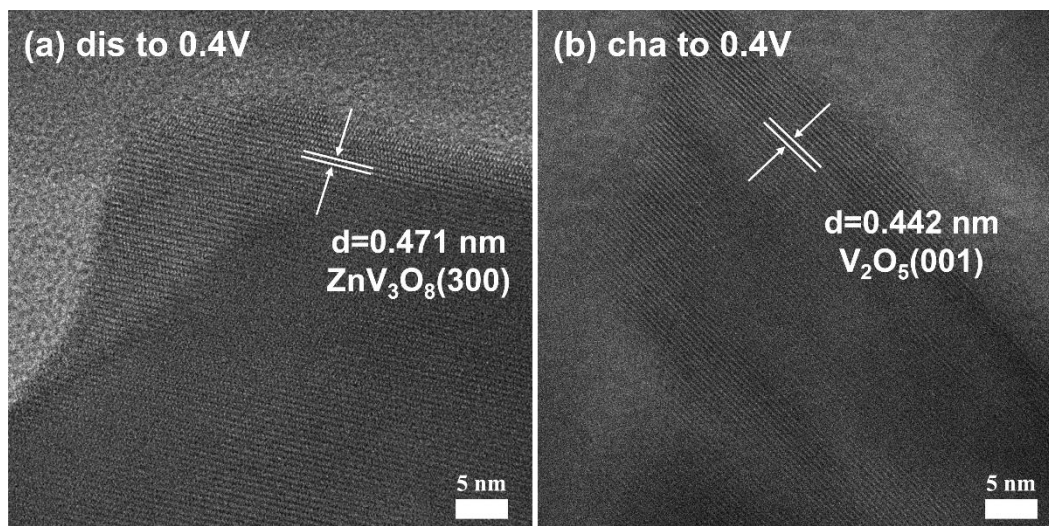


Figure S12. The pictures of battery separators after different recycle times: (a) 1st, (b) 10th, (c) 100th and (d) 500th.



**Figure S13.** HRTEM images of  $V_2O_5$ -20 electrode (a) discharged to 0.4 V, (b) charged to 1.4 V.

**Table S1.** The BET surface area, pore volume and average pore size of  $V_2O_5$ -0 nanoparticles and  $V_2O_5$ -0 microspheres samples.

Sample	BET surface area ( $m^2g^{-1}$ )	Pore volume ( $cm^3 g^{-1}$ )	Average pore diameter(nm)
$V_2O_5$ -0	6.8468	0.03272	10.1882
$V_2O_5$ -20	9.4024	0.04763	37.0358

**Table S2.** A survey of  $V_2O_5$ -based electrode materials with three-dimensional structures for AZIBs.

Cathode material [Structure characteristic]	Electrolyte	Specific capacity	Cycling performance	Reference.
$V_2O_5$ (porous microspheres)	3M $Zn(CF_3SO_3)_2$	401mAh/g (0.1 A/g)	73% (1000) (2A/g)	[15]
$V_2O_5$ (hollow spheres)	Saturated $ZnSO_4$	280mAh/g (0.2 A/g)	82% (6200) (10A/g)	[22]
$V_2O_5$ (nanospheres)	3M $ZnSO_4$	327mAh/g (0.1 A/g)	69% (6000) (10A/g)	[41]
$V_2O_5@CNTs$ (irregular spherical)	1 M $ZnSO_4/1 Na_2SO_4$	293mAh/g (0.3 A/g)	72% (6000) (5A/g)	[42]
$VO_2$ (hollow nanospheres)	3M $Zn(CF_3SO_3)_2$	440mAh/g (0.1 A/g)	47% (860) (1A/g)	[43]